Estimates of nasal airflow at the nasal cycle mid-point improve the correlation between objective and subjective measures of nasal patency

Courtney Gaberino[1,2], **John S. Rhee**[1], and **Guilherme J.M. Garcia**[1,2]

[1]Department of Otolaryngology and Communication Sciences, Medical College of Wisconsin

[2]Department of Biomedical Engineering, Medical College of Wisconsin

Abstract

INTRODUCTION—The nasal cycle represents a significant challenge when comparing pre- and post-surgery objective measures of nasal airflow.

METHODS—Computational fluid dynamics (CFD) simulations of nasal airflow were conducted in 12 nasal airway obstruction patients showing significant nasal cycling between pre- and post-surgery computed tomography scans. To correct for the nasal cycle, mid-cycle models were created virtually. Subjective scores of nasal patency were obtained via the Nasal Obstruction Symptom Evaluation (NOSE) and unilateral visual analog scale (VAS).

RESULTS—The correlation between objective and subjective measures of nasal patency increased after correcting for the nasal cycle. In contrast to biophysical variables in individual patients, cohort averages were not significantly affected by the nasal cycle correction.

CONCLUSIONS—The ability to correct for the confounding effect of the nasal cycle is a key element that future virtual surgery planning software for nasal airway obstruction will need to account for when using anatomic models based on single instantaneous imaging.

Keywords

nasal cycle correction; nasal airway obstruction; nasal resistance; mucosal cooling; computational fluid dynamics (CFD) simulations; virtual surgery planning

1. Introduction

There is much interest in the development of a virtual surgery tool to optimize the outcomes of nasal airway obstruction (NAO) surgery. Currently, surgical planning for NAO patients

relies on subjective symptoms, physical exam findings, and physician judgment without any objective measurements. In theory, a virtual surgery software tool based on computational fluid dynamics (CFD) simulations of nasal airflow can be developed to identify which patients would benefit the most from surgery and to select the optimal surgical procedure for each patient (Hariri et al., 2015; Rhee et al., 2011). This virtual surgery tool will most likely rely on instantaneous imaging (computed tomography scans or magnetic resonance imaging) to capture an individual's nasal anatomy. Therefore, a key challenge for future virtual surgery tools is the need to account for the spontaneous fluctuation in nasal mucosa engorgement known as the "nasal cycle" (Eccles, 2000; Patel et al., 2015; Quine et al., 1999).

In the classical nasal cycle, unilateral airflow switches between the left and right nostrils every 2–3 hours in the absence of any external stimuli, while bilateral airflow remains approximately constant (Eccles, 2000; Hasegawa and Kern, 1978). However, some patients exhibit different patterns of spontaneous fluctuations, including non-reciprocal and/or non-cyclical airflow fluctuations (Flanagan and Eccles, 1997). For this reason, a single snapshot of a patient's nasal passage does not always reflect the average airflow the patient experiences during her/his daily activities. Our group recently reported a methodology to simulate the nasal cycle and quantify flow variables at the mid-cycle point (Patel et al., 2015). The method requires the creation of multiple nasal cycle models for each surgical state (i.e., pre-surgery and post-surgery), running CFD simulations in each model, and fitting a curve to describe the relationship between flow variables and inferior turbinate thickness so that flow variables can be estimated at the mid-cycle. This method was previously applied to simulate the nasal cycle in two NAO patients and the results revealed that the nasal cycle can dramatically influence objective measures of surgical outcomes (Garcia et al., 2015a; Patel et al., 2015).

The nasal cycle needs to be accounted for when quantifying changes in objective measures after NAO surgery. The method described in our previous study (Patel et al., 2015) was very labor-intensive due to the requirement to create multiple models for each surgical state, which prevented the analysis of a larger sample size. In the present paper, we describe an alternative strategy that requires the creation of a single pre-surgery mid-cycle model and a single post-surgery mid-cycle model. This new method is much faster to perform, but it was unclear whether the two methods would provide equivalent results. Here, we demonstrate that the two methods provide similar results, which allowed us to investigate a larger cohort of 12 cycling NAO patients. Our results reveal that the correlation between airflow variables and subjective nasal patency is higher after correcting for the nasal cycle.

2. Methods

2.1- Patient Selection

This project was approved by the Medical College of Wisconsin's IRB committee and each patient gave informed consent. This manuscript is part of a larger study investigating the correlation between subjective and objective measures of nasal airflow (Dayal et al., 2016; Frank-Ito et al., 2014; Garcia et al., 2016; Hariri et al., 2015; Kimbell et al., 2013; Patel et al., 2015; Rhee et al., 2014; Sullivan et al., 2014). The cohort consisted of 27 patients all

undergoing surgery to treat chronic nasal airway obstruction (septoplasty, turbinectomy, and/or functional rhinoplasty). For each patient, a single set of pre- and post-operative CT scans were obtained with 0.6mm increments and in-plane resolution of 0.31mm.

Patients exhibiting significant nasal cycle between pre- and post-surgery scans were selected based on changes in mucosal engorgement, as follows. A relative distance along the nasal cavity was defined as $D = z/L_{septum}$, where z is the distance from the nostrils and L_{septum} is the septum length from nostrils to nasal choana (Figure 1). The cross-sectional area (CSA) of the inferior turbinate was averaged over five uniformly-spaced coronal sections located at distances $0.5 \leq D \leq 0.9$ (Figure 2). (Sections in the anterior nose were not used because several patients underwent turbinate reduction that was limited to the anterior nose.) The percentage change in CSA between pre- and post-surgery scans was defined as $Percent\ Change = 100 \times |CSA_{POST} - CSA_{PRE}|/CSA_{PRE}$ for each nasal cavity in each patient. Patients with percent changes in mucosal engorgement greater than 15% were defined to have significant nasal cycle differences between the pre- and post-surgery scans. Based on this criterion, 12 out of the 27 patients were identified as requiring a nasal cycle correction.

2.2 - Subjective scores of nasal patency

Patients were administered the Nasal Obstruction Symptom Evaluation (NOSE) to collect information on subjective symptoms before and after surgery (Stewart et al., 2004a). The NOSE scale is a disease-specific quality-of-life instrument for NAO that has been validated for septoplasty and nasal valve repair, and is used to measure surgical success (Rhee et al., 2014; Stewart et al., 2004b; Stewart et al., 2004a). The NOSE scale was selected because (a) it is simple and quick, (b) it is the quality-of-life (QOL) instrument most frequently used to assess surgical outcomes in NAO, and (c) it is more specific for NAO than other rhinological QOL instruments (Hopkins, 2009). It is a five item scale where each patient scores, over the past month, their symptoms of nasal congestion, nasal blockage, trouble breathing through the nose, trouble sleeping, and air hunger sensation using a scale from 0 (not a problem) to 4 (severe problem). These numbers are summed and multiplied by 5 to give a score that ranges from 0 (no symptoms) to 100 (severe symptoms).

Unilateral visual analog scale (VAS) scores for nasal airflow were also collected before and after surgery. Patients were asked to cover one nostril and rate their ability to breathe through the uncovered nostril on a scale of 1 (completely obstructed) to 10 (no obstruction). The VAS score was a subjective measure of instantaneous airflow at the time of consultation, while the NOSE score was used to assess the symptoms of nasal obstruction during the past month. For each patient, either the left cavity or the right cavity was assigned as the most obstructed side based on the pre-surgery VAS scores.

2.3 - Creation of Pre- and Post-Surgical Models

Three-dimensional (3D) models of the pre-surgery and post-surgery nasal anatomy were created for each patient in Mimics™ 16.0 (Materialise Inc., Leuven, Belgium) based on the CT scans. The nasal passage extended from the nostrils to the nasopharynx while excluding the paranasal sinuses. Consistent borders along the sinus ostia between pre- and post-surgical models were obtained by co-registering the models based on facial bones.

2.4 - Creation of Nasal Cycle Models

Nasal cycle models were created for both surgical states (i.e., pre-surgery and post-surgery) using the Morphology Operations tool in Mimics™ (Figure 3). This tool allows users to erode or dilate masks by an integer number of pixels. Using this tool, the airspace around the inferior and middle turbinates was reduced/expanded to reproduce the effect of mucosal congestion/decongestion (Figure 3). When creating the pre-surgery batch of nasal cycle models, the post-surgery anatomy was used as a limit, so that the nasal cycle models stayed within the range of mucosal congestion/decongestion depicted in the CT scans. In other words, it was assumed that the pre- and post-surgery CT scans depicted the extremes of mucosal congestion/decongestion in each patient. Similarly, when creating the post-surgery batch of nasal cycle models, the pre-surgery anatomy was used as a limit to morphological changes of the airspace surrounding the inferior and middle turbinates.

2.5 - Computational Fluid Dynamics (CFD) Simulations

Biophysical measures of nasal airflow were quantified using computational fluid dynamics (CFD) using methods previously described (Garcia et al., 2007; Kimbell et al., 2013; Sullivan et al., 2014). Briefly, the nasal models were meshed with approximately 4 million tetrahedral cells in ICEM-CFD 14.0 (ANSYS, Inc, Canonsburg, Pennsylvania). The steady-state Navier-Stokes equations were solved in Fluent 14.0 (ANSYS, Inc) assuming laminar flow. The following boundary conditions were used: (1) gauge pressure at the inlet (nostrils) = 0 Pa, (2) air velocity at the walls = 0 m/s, and (3) a patient-specific outlet pressure. The post-surgery outlet pressure was such that the inhalation rate expected based on body mass (see below) was achieved. The pre-surgery outlet pressure was such that the transnasal pressure drop (nostrils to choana) was the same in the pre- and post-surgery models. This is important because the soft palate can have different configurations in the pre- and post-surgery scans leading to different nasopharynx resistances in the pre- and post-surgery models, which can confound the results when the same outlet pressure is imposed on all models (Borojeni et al., 2016; Kim et al., 2013). In other words, inhalation rates were different in the pre- and post-surgery models, but the pressure drop (nostrils to choana) was the same in each subject.

The post-surgery inhalation rate was estimated from gender-specific allometric curves that relate minute volume ($\dot{V}_E$) to body mass (M) (Garcia et al., 2009):

$$\text{Males (sitting awake):} \quad \dot{V}_E = (1.36 \pm 0.10) M^{0.44 \pm 0.02}$$

$$\text{Females (sitting awake):} \quad \dot{V}_E = (1.89 \pm 0.40) M^{0.32 \pm 0.06}$$

where $\dot{V}_E$ is in liters per minute (L/min) and M is in kilograms (kg). The steady-state inhalation rate is twice the minute volume. The heat transfer simulations assumed that air temperature was T=20°C at the nostrils and T=32.6°C at the nasal mucosa, which corresponds to the average nasal mucosal temperature during inspiration as reported by (Lindemann et al., 2002).

2.6 - Outcome Measures

In this manuscript, we focus on unilateral CFD variables in the most obstructed side based on previous reports that: (1) subjective nasal patency has a stronger correlation with unilateral rather than bilateral measures (Andre et al., 2009), and (2) subjective nasal patency has a stronger correlation with unilateral measures in the most obstructed side than with measures in the least obstructed side (Kimbell et al., 2013). An analysis of the correlation between NOSE and VAS scores in our cohort supports the hypothesis that subjective nasal patency is more associated with airflow in the most obstructed side than airflow in the least obstructed side. The NOSE scale is by definition a bilateral scale, while a unilateral VAS was used in this study. In our cohort of 12 patients, a much stronger correlation was found between NOSE and VAS in the most obstructed side (Spearman r= −0.88, p=1×10^{-8}) than between NOSE and VAS in the least obstructed side (Spearman r= −0.52, p=0.009) (see Figure S1 in the Supplementary Material). Therefore, all CFD variables reported in this manuscript are unilateral values in the most obstructed side, except for the last subsection in the Results (section 3.6), where bilateral variables are presented.

The biophysical measures of nasal airflow computed in this study include the nasal resistance (R), airflow rate (Q), total heat flux (HF), and surface area stimulated by mucosal cooling. Nasal resistance is defined as the ratio of the transnasal pressure drop (nostrils to choana) to airflow rate (R = P/Q). Total heat flux is calculated as the rate of heat loss from the nasal mucosa to inspired air between nostrils and nasal choana divided by the corresponding surface area (Kimbell et al., 2013; Sullivan et al., 2014).

Previous studies have shown that subjective nasal patency correlates with mucosal cooling during inspiration (Kimbell et al., 2013; Sullivan et al., 2014; Zhao et al., 2011; Zhao et al., 2014). This leads to the question of how to quantify mucosal cooling. Zhao and colleagues proposed that mucosal cooling can be quantified by the peak heat flux posterior to the nasal vestibule (Zhao et al., 2014). Our group proposed that mucosal cooling should be quantified as the surface area stimulated by mucosal cooling (Sullivan et al., 2014). This is based on experimental data suggesting that menthol-sensitive cold-receptors are uniformly distributed on the nasal mucosa (Liu et al., 2015; Meusel et al., 2010). In our previous study of 10 NAO patients with symmetrical mucosal engorgement in both the pre- and post-surgery CT scans, we found that the surface area where heat flux exceeds 50 W/m^2 (SAHF50) had the strongest correlation with patency scores. The threshold 50 W/m^2 was selected as the value that maximized the correlation between subjective patency scores and CFD-derived mucosal cooling (Sullivan et al., 2014). This threshold corresponded to a large region of the nasal mucosa, rather than a localized region where heat flux reaches a peak (Figure S2).

2.7 - Mid-Cycle Surgical Effect

The mid-cycle surgical effect was calculated with two methods. Both methods assumed that the pre- and post-surgery CT scans depicted the nasal anatomy at opposite extremes of the nasal cycle.

2.7.1 - Method 1—Following Patel's method, for five of the twelve nasal cycling patients a series of nasal cycling models were created to represent gradual changes in mucosal

engorgement due to the nasal cycle (Patel et al., 2015). Including the pre- and post-surgery models, a total of 39 CFD models were developed for these five patients. To estimate mid-cycle objective measures of nasal patency, flow variables were plotted against the average inferior turbinate CSA. A third order polynomial curve was fit to the data points and the mid-cycle value was estimated based on the fitting curves (Figure 4A). The mid-cycle point was determined based on the average inferior turbinate CSA in the posterior half of the turbinate, where no surgical changes were made. Thus, the mid-cycle surgical effect was the difference between the pre-surgery nasal cycle curve and post-surgery nasal cycle curve at the mid-cycle inferior turbinate CSA (Figure 4A).

2.7.2 - Method 2—For all twelve cycling patients a single mid-cycle pre-surgery model and a single mid-cycle post-surgery model were created. After co-registering the pre- and post-surgery models within Mimics, the airspace was dilated/eroded until a best approximated mid-cycle point was determined throughout the length of the turbinates. This was done for both the pre-surgery anatomy and the post-surgery anatomy, resulting in 2 mid-cycle models for each patient. Given that the airspace dilation/erosion could be performed only in integer number of pixels, the inferior turbinate CSA in the mid-cycle models approximated, but was not exactly equal to, the average inferior turbinate CSA (Figure 4B). The mid-cycle surgical effect was defined as the difference between the mid-cycle pre-surgery model and the mid-cycle post-surgery model (Figure 4B). Including pre- and post-surgery models, a total of 48 CFD models were developed for the twelve patients (4 models for each patient).

2.7.3 - Comparing Method 1 vs. Method 2—The surgical effect was computed as $\Delta V = V_{POST} - V_{PRE}$, where V_{POST} and V_{PRE} are the post-surgery and pre-surgery values for a given variable V, respectively. To compare Methods 1 and 2, the percent difference between Methods 1 and 2 was estimated as

$$\text{Percent Difference} = 100 \left| \frac{\Delta V_{\text{METHOD } 1} - \Delta V_{\text{METHOD } 2}}{\Delta V_{\text{METHOD } 1}} \right|. \quad (1)$$

where $\Delta V_{METHOD\,1}$ and $\Delta V_{METHOD\,2}$ are the surgical changes estimated with Methods 1 and 2, respectively. A Bland Altman analysis was also used to compare the two methods (Giavarina, 2015).

Statistical analysis

Wilcoxon signed rank tests (paired, two-sided) were used to test whether differences between pre-surgery and post-surgery variables were statistically significant at the level $p < 0.05$. Both the Spearman correlation coefficient and the Pearson's correlation coefficient were used to quantify the correlation between CFD variables and subjective nasal patency scores.

3. Results

3.1 - Subjective patency scores

NOSE and VAS scores improved after surgery in all 12 subjects. The NOSE scores decreased from 64 ± 20 pre-surgery to 16 ± 14 post-surgery (p=0.0005). Similarly, VAS scores increased from 3.3 ± 2.1 pre-surgery to 8.4 ± 1.6 post-surgery in the most obstructed side (p=0.0005). On the least obstructed side the VAS scores were not significantly changed after surgery (7.5 ± 2.4 pre-surgery vs. 8.3 ± 2.1 post-surgery, p=0.36).

3.2 - Comparison of Method 1 and Method 2

Methods 1 and 2 provided very similar estimates of the surgical effect in the five patients in which both methods were performed (Figure 5 and Table 1). The average pre-surgery to post-surgery changes in CFD variables in this 5-patient cohort were as follows: R = -0.08 ± 0.12 Pa.s/ml and -0.08 ± 0.12 Pa.s/ml for methods 1 and 2, respectively;   Q = 36 ± 34 ml/s and 38 ± 36 ml/s for methods 1 and 2, respectively;   HF = 40 ± 51 W/m^2 and 42 ± 50 W/m^2 for methods 1 and 2, respectively; and   SAHF50 = 6 ± 10 cm^2 and 5 ± 10 cm^2 for methods 1 and 2, respectively (Figure 5). The Bland Altman analysis also suggested that the two methods were equivalent because the confidence interval of the mean difference between Method 1 and Method 2 included the zero for all CFD variables studied (see Figure S3 in the Supplementary Material). Due to such minimal difference between the two methods, Method 2 was subsequently used to examine the effect of nasal cycling corrections on the twelve patient cohort.

3.3 - Average surgical changes in objective variables

The CFD simulations revealed a statistically significant improvement in all flow variables in the 12-patient cohort (Figure 6 and Table 2). Nasal resistance decreased post-surgery, which led to an increase in unilateral airflow, an increase in the average heat flux, and an increase in the surface area stimulated by mucosal cooling in the nasal cavity that was most obstructed pre-operatively (Figure 6). The post-surgical improvement was statistically significant for all CFD variables both before and after correcting for the nasal cycle, except that the surgical change in SAHF50 was not statistically significant before the nasal cycle correction (Table 2). The nasal cycle correction did not affect the average CFD variables substantially (Table 2).

3.4 - Surgical changes in individual patients

Although the nasal cycle correction had a minor impact on the cohort average CFD variables, the surgical effect estimated for individual patients was affected by the nasal cycle correction. As illustrated in Figure 7, the surgical effect in individual patients increased, decreased, or did not change after correcting for the nasal cycle. For the 12 patients investigated, the surgical effect increased in 5 patients, decreased in 4 patients, and remained relatively unchanged in 3 patients after the nasal cycle correction.

3.5 - Correlation between CFD variables and subjective nasal patency

Before correcting for the nasal cycle, the only correlation between subjective and objective measures of nasal airflow was found between NOSE score and flowrate (Spearman r = −0.41, p = 0.048) (Table 3). After correcting for the nasal cycle, all CFD variables had a statistically significant correlation with both NOSE and VAS scores, except that SAHF50 did not correlate with VAS (Table 3). The CFD variables with the strongest correlation with subjective scores after the nasal cycle correction were flowrate (Spearman r = −0.61, p = 0.002 with NOSE; Spearman r = 0.56, p = 0.004 with VAS) and nasal resistance (Spearman r = 0.55, p = 0.005 with NOSE; Spearman r = −0.58, p = 0.003 with VAS) (Table 3). Importantly, besides increasing both the Spearman and Pearson correlation coefficients, correcting for the nasal cycle narrowed the 95% confidence intervals of the Pearson correlation coefficients, which support the conclusion that correcting for the nasal cycle strengthens the correlation between subjective and objective measures of nasal airflow (Table S1).

3.6 - Bilateral CFD variables

Mean bilateral CFD variables pre- and post-surgery are presented in the Supplementary Material. Statistically significant post-surgical improvement was observed in bilateral resistance, bilateral flowrate, and bilateral heat flux, but not in bilateral SAHF50 (Table S2). The nasal cycle correction using Method 2 did not change substantially the cohort average CFD variables (Table S2). Before correcting for the nasal cycle, there were no statistically significant correlations between bilateral CFD variables and subjective patency scores (Table S3). After correcting for the nasal cycle, two correlations became statistically significant, namely NOSE vs. bilateral flowrate, and VAS vs. bilateral SAHF50 (Table S3). Importantly, subjective nasal patency had a higher correlation with unilateral than with bilateral CFD variables (compare Table 3 and Table S3), which is consistent with previous studies (Andre et al., 2009; Kimbell et al., 2013).

4. Discussion

In recent years, CFD technology has been increasingly applied to quantify nasal physiology. Researchers have explored a myriad of topics, such as characterizing nasal airflow in healthy subjects (Zhao and Jiang, 2014), quantifying nasal filtration of airborne particles (Frank-Ito et al., 2015; Garcia et al., 2015b; Schroeter et al., 2011; Schroeter et al., 2015), heating and humidification of inspired air (Dayal et al., 2016; Goodarzi-Ardakani et al., 2016), the relationship between nasal function and nasal anatomy (Garcia et al., 2016; Patki and Frank-Ito, 2016), and airflow in the paranasal sinuses (Zhu et al., 2012; Zhu et al., 2014). In particular, there is much interest in identifying flow variables that correlate with symptoms of nasal airway obstruction (Garcia et al., 2016; Garcia et al., 2010; Hariri et al., 2015; Kim et al., 2014; Na et al., 2012). Experimental studies suggest that mucosal cooling by inspired air plays a key role in nasal airflow sensation (Bailey et al., 2016; Burrow et al., 1983; Eccles et al., 1988; Sozansky and Houser, 2014; Zhao et al., 2011), thus rendering CFD technology a suitable technology to quantify heat transfer and mucosal cooling. Indeed, studies from our group demonstrated that CFD-derived nasal airflow, nasal resistance, heat flux, and the surface area stimulated by mucosal cooling (SAHF50) correlate with patients'

subjective feelings of nasal obstruction (Kimbell et al., 2013; Sullivan et al., 2014). Altogether, these studies suggest that CFD technology may become the basis for a virtual surgery tool for optimizing NAO surgical outcomes. However, the fluctuations in mucosal engorgement associated with the nasal cycle represent a major challenge for virtual surgery planning based on a single instantaneous imaging that captures a snapshot of nasal anatomy.

To date, few studies have investigated how the nasal cycle affects objective measures of nasal airflow before and after nasal surgery. Quine and colleagues used posterior rhinomanometry to study the effect of the nasal cycle in 27 chronic rhinitis patients undergoing inferior turbinate reduction via submucosal diathermy (Quine et al., 1999). The median bilateral nasal airflow measured at a transnasal pressure drop of 75 Pa increased from 246 ml/s pre-surgery to 371 ml/s post-surgery, demonstrating objectively the benefit of submucosal diathermy. The minimum unilateral nasal airflow (Fmin) during the nasal cycle increased from a median of 69 ml/s pre-surgery to 163 ml/s post-surgery, while the maximum unilateral airflow (Fmax) increased from a median of 171 ml/s pre-surgery to 211 ml/s post-surgery. The greater increase in Fmin as compared to Fmax led the authors to conclude that submucosal diathermy reduced the amplitude of the nasal cycle, inducing the mucosa to be in a state of relative vasoconstriction, thus increasing nasal airflow (Quine et al., 1999).

Patel and colleagues (Patel et al., 2015) used CFD to study the effect of changes in mucosal engorgement on nasal airflow variables in two NAO patients. Using virtual surgery (Method 1), the authors demonstrated that the nasal cycle can dramatically influence objective measures of surgical outcomes. Due to the labor-intensive nature of creating multiple nasal cycle models for each patient, the analysis was limited to 2 patients. Jo and colleagues also studied changes in nasal aerodynamics during the nasal cycle (Jo et al., 2015). After reviewing a cohort of 32 patients with symptoms of nasal obstruction, two patients with chronic rhinosinusitis were selected who had obvious reciprocal changes in mucosal engorgement between two sets of CT scans. The authors presented a detailed analysis of how the nasal cycle affected airspace cross-sectional areas, air velocity, pressure distribution, and local nasal resistance. The two patients exhibited very different behaviors. In Patient 1, the minimal cross-sectional area was located at the internal nasal valve, thus the distribution of local resistances shifted dramatically when mucosal engorgement changed due to the nasal cycle. In contrast, in Patient 2, the nostrils were the most constricted region of the nasal cavity, consequently the distribution of local resistances was relatively unchanged during the nasal cycle. To our knowledge, these two studies are the only publications that have applied CFD technology to investigate how the nasal cycle affects nasal aerodynamics.

Our study contributes to this literature by providing an effective virtual surgery strategy to account for the nasal cycle when quantifying nasal function pre- and post-surgery. We found that creation of a single mid-cycle model (Method 2) provided similar results as the more labor-intensive method developed by Patel and colleagues (Method 1) (Figures 4, 5, and S3). In previous studies from our group (Frank-Ito et al., 2014; Kimbell et al., 2013; Sullivan et al., 2014), the confounding effect of the nasal cycle was avoided by removing from the study patients who had asymmetrical mucosal engorgement in the left and right cavities. This strategy limited our sample size. Thus, the methodology presented in this study will allow

the analysis of larger cohorts of patients. A major finding of this study is that correcting for the nasal cycle increased the correlation between objective and subjective measures of nasal airflow (Figure 8, Table 3, and Table S3), which confirms the importance of accounting for the nasal cycle. Interestingly, cohort averages were not substantially affected by the nasal cycle correction (Figure 6, Table 2, and Table S2), but objective measures of the surgical effect in individual patients were affected by the nasal cycle correction (Figure 7).

Some limitations of this study must be acknowledged. First, it was assumed that pre- and post-operative CT scans were obtained at opposite extremes of the nasal cycle. This assumption is supported by in vivo measurements showing that the transition between cycling states is rapid compared to the amount of time spent at either cycling extreme (Grutzenmacher et al., 2005). Second, our nasal cycle models did not account for mucosal changes along the nasal floor, superior turbinates, or nasal septum due to difficulty constructing consistent changes. Third, the mask dilation or erosion was performed in integer number of pixels due to limitations in the Mimics software. Thus, Method 2 represents an approximation of the mid-cycle point, rather than exactly the mid-cycle point. Fourth, the use of the post-operative CT scan for data analysis used in this cohort is limited to research groups because post-operative CT scans are not routinely obtained. Fifth, this study is purely computational and experimental measurements of airflow were not available to validate our numerical predictions. Finally, it must be acknowledged that even after correcting for the nasal cycle, the highest Pearson correlation coefficient was $|r| = 0.63$ (Table S1), which provides a coefficient of determination $r^2 = 0.40$, thus our CFD variables explain only about 40% of the variance in the subjective scores. This relatively low coefficient of determination may not be due to our methods, but rather may signal an inherent difficulty of explaining subjective sensations, given that studies correlating dyspnea and spirometry have reported similar coefficients of determination (Martinez-Garcia et al., 2007). Despite these limitations, we believe that our results shed some light on how the nasal cycle can affect objective measures of nasal airflow. Also, we believe our methodology will be useful to other researchers interested in virtual surgery planning using CFD models, which inherently are based on instantaneous medical images that do not capture the nasal cycle.

5. Conclusion

In summary, this was the first time that nasal cycling effects were evaluated using CFD technology in a large cohort of patients. We found that building one mid-cycle model provided similar results to creating multiple nasal cycle models, thus providing a more efficient methodology that can be applied in larger cohorts. We found that a nasal cycle correction is required to evaluate surgical changes in individual patients. In contrast, cohort averages were not substantially affected by the nasal cycle correction. Importantly, the correlation between subjective and objective measures of nasal airflow increased after correcting for the nasal cycle, suggesting that flow variables evaluated at mid-cycle are more representative of a patients' perception of nasal patency. We conclude that the nasal cycle can have a significant impact on objective measures of nasal airflow, and that it is important that future virtual surgery planning software account for the nasal cycle.

Supplementary Material

Refer to Web version on PubMed Central for supplementary material.

Acknowledgments

References

Andre RF, Vuyk HD, Ahmed A, Graamans K, Nolst Trenite GJ. Correlation between subjective and objective evaluation of the nasal airway. A systematic review of the highest level of evidence. Clin. Otolaryngol. 2009; 34:518–525. [PubMed: 20070760]

Bailey RS, Casey KP, Pawar SS, Garcia GJM. Nasal mucosal temperature and its potential correlation to subjective nasal patency in healthy individuals. JAMA Facial Plast Surg. 2016

Borojeni AAT, Frank-Ito DO, Kimbell JS, Rhee JS, Garcia GJ. Creation of an idealized nasopharynx geometry for accurate computational fluid dynamics simulations of nasal airflow in patient-specific models lacking the nasopharynx anatomy. International journal for numerical methods in biomedical engineering. 2016

Burrow A, Eccles R, Jones AS. The effects of camphor, eucalyptus and menthol vapour on nasal resistance to airflow and nasal sensation. Acta Otolaryngol. 1983; 96:157–161. [PubMed: 6613544]

Dayal A, Rhee JS, Garcia GJM. Impact of Middle vs. Inferior Total Turbinectomy on Nasal Aerodynamics. Otolaryngol Head and Neck Surg. 2016; 155:518–525. [PubMed: 27165673]

Eccles R. Nasal airflow in health and disease. Acta Otolaryngol. 2000; 120:580–595. [PubMed: 11039867]

Eccles R, Griffiths DH, Newton CG, Tolley NS. The effects of menthol isomers on nasal sensation of airflow. Clin. Otolaryngol. Allied Sci. 1988; 13:25–29. [PubMed: 3370851]

Flanagan P, Eccles R. Spontaneous changes of unilateral nasal airflow in man. A re-examination of the 'nasal cycle'. Acta Otolaryngol. 1997; 117:590–595. [PubMed: 9288218]

Frank-Ito DO, Kimbell JS, Laud P, Garcia GJ, Rhee JS. Predicting postsurgery nasal physiology with computational modeling: current challenges and limitations. Otolaryngol. Head Neck Surg. 2014; 151:751–759. [PubMed: 25168451]

Frank-Ito DO, Wofford M, Schroeter JD, Kimbell JS. Influence of Mesh Density on Airflow and Particle Deposition in Sinonasal Airway Modeling. J. Aerosol Med. Pulm. Drug Deliv. 2015; 29:46–56.

Garcia GJ, Bailie N, Martins DA, Kimbell JS. Atrophic rhinitis: a CFD study of air conditioning in the nasal cavity. J. Appl. Physiol. 2007; 103:1082–1092. [PubMed: 17569762]

Garcia GJ, Hariri BM, Patel RG, Rhee JS. The relationship between nasal resistance to airflow and the airspace minimal cross-sectional area. J. Biomech. 2016; 49:1670–1678. [PubMed: 27083059]

Garcia GJ, Patel RG, Frank-Ito DO, Kimbell JS, Rhee JS. Response to Dr Chung's Question on Simulating the Nasal Cycle with Computational Fluid Dynamics. Otolaryngol. Head Neck Surg. 2015a; 153:308–309.

Garcia GJ, Rhee JS, Senior BA, Kimbell JS. Septal deviation and nasal resistance: an investigation using virtual surgery and computational fluid dynamics. American journal of rhinology & allergy. 2010; 24:e46–e53. [PubMed: 20109325]

Garcia GJ, Schroeter JD, Kimbell JS. Olfactory deposition of inhaled nanoparticles in humans. Inhal. Toxicol. 2015b; 27:394–403. [PubMed: 26194036]

Garcia GJM, Schroeter JD, Segal RA, Stanek J, Foureman GL, Kimbell JS. Dosimetry of nasal uptake of water-soluble and reactive gases: A first study of interhuman variability. Inhalation Toxicology. 2009; 21:607–618. [PubMed: 19459775]

Giavarina D. Understanding Bland Altman analysis. Biochem. Med. (Zagreb). 2015; 25:141–151. [PubMed: 26110027]

Goodarzi-Ardakani V, Taeibi-Rahni M, Salimi MR, Ahmadi G. Computational simulation of temperature and velocity distribution in human upper respiratory airway during inhalation of hot air. Respir. Physiol. Neurobiol. 2016; 223:49–58. [PubMed: 26777422]

Grutzenmacher S, Lang C, Mlynski R, Mlynski B, Mlynski G. Long-term rhinoflowmetry: a new method for functional rhinologic diagnostics. Am. J. Rhinol. 2005; 19:53–57. [PubMed: 15794075]

Hariri BM, Rhee JS, Garcia GJ. Identifying patients who may benefit from inferior turbinate reduction using computer simulations. Laryngoscope. 2015; 125:2635–2641. [PubMed: 25963247]

Hasegawa M, Kern EB. Variations in nasal resistance in man: a rhinomanometric study of the nasal cycle in 50 human subjects. Rhinology. 1978; 16:19–29. [PubMed: 635366]

Hopkins C. Patient reported outcome measures in rhinology. Rhinology. 2009; 47:10–17. [PubMed: 19382488]

Jo G, Chung SK, Na Y. Numerical study of the effect of the nasal cycle on unilateral nasal resistance. Respir. Physiol. Neurobiol. 2015; 219:58–68. [PubMed: 26315663]

Kim SK, Heo GE, Seo A, Na Y, Chung SK. Correlation between nasal airflow characteristics and clinical relevance of nasal septal deviation to nasal airway obstruction. Respir. Physiol. Neurobiol. 2014; 192:95–101. [PubMed: 24361464]

Kim SK, Na Y, Kim JI, Chung SK. Patient specific CFD models of nasal airflow: overview of methods and challenges. J. Biomech. 2013; 46:299–306. [PubMed: 23261244]

Kimbell JS, Frank DO, Laud P, Garcia GJ, Rhee JS. Changes in nasal airflow and heat transfer correlate with symptom improvement after surgery for nasal obstruction. J. Biomech. 2013; 46:2634–2643. [PubMed: 24063885]

Liu SC, Lu HH, Cheng LH, Chu YH, Lee FP, Wu CC, Wang HW. Identification of the cold receptor TRPM8 in the nasal mucosa. American journal of rhinology & allergy. 2015; 29:e112–e116. [PubMed: 26163239]

Martinez-Garcia MA, Perpina-Tordera M, Soler-Cataluna JJ, Roman-Sanchez P, Lloris-Bayo A, Gonzalez-Molina A. Dissociation of lung function, dyspnea ratings and pulmonary extension in bronchiectasis. Respir. Med. 2007; 101:2248–2253. [PubMed: 17698334]

Meusel T, Negoias S, Scheibe M, Hummel T. Topographical differences in distribution and responsiveness of trigeminal sensitivity within the human nasal mucosa. Pain. 2010; 151:516–521. [PubMed: 20817356]

Na Y, Chung KS, Chung SK, Kim SK. Effects of single-sided inferior turbinectomy on nasal function and airflow characteristics. Respir. Physiol. Neurobiol. 2012; 180:289–297. [PubMed: 22227321]

Patel RG, Garcia GJ, Frank-Ito DO, Kimbell JS, Rhee JS. Simulating the nasal cycle with computational fluid dynamics. Otolaryngol. Head Neck Surg. 2015; 152:353–360. [PubMed: 25450411]

Patki A, Frank-Ito DO. Characterizing human nasal airflow physiologic variables by nasal index. Respir. Physiol. Neurobiol. 2016; 232:66–74. [PubMed: 27431449]

Quine SM, Aitken PM, Eccles R. Effect of submucosal diathermy to the inferior turbinates on unilateral and total nasal airflow in patients with rhinitis. Acta Otolaryngol. 1999; 119:911–915. [PubMed: 10728933]

Rhee JS, Pawar SS, Garcia GJ, Kimbell JS. Toward personalized nasal surgery using computational fluid dynamics. Arch. Facial Plast. Surg. 2011; 13:305–310. [PubMed: 21502467]

Rhee JS, Sullivan CD, Frank DO, Kimbell JS, Garcia GJ. A systematic review of patient-reported nasal obstruction scores: defining normative and symptomatic ranges in surgical patients. JAMA facial plastic surgery. 2014; 16:219–225. quiz 232. [PubMed: 24604253]

Schroeter JD, Garcia GJ, Kimbell JS. Effects of Surface Smoothness on Inertial Particle Deposition in Human Nasal Models. Journal of aerosol science. 2011; 42:52–63. [PubMed: 21339833]

Schroeter JD, Tewksbury EW, Wong BA, Kimbell JS. Experimental measurements and computational predictions of regional particle deposition in a sectional nasal model. J. Aerosol Med. Pulm. Drug Deliv. 2015; 28:20–29. [PubMed: 24580111]

Sozansky J, Houser SM. The physiological mechanism for sensing nasal airflow: a literature review. International forum of allergy & rhinology. 2014; 4:834–838. [PubMed: 25079504]

Stewart MG, Smith TL, Weaver EM, Witsell DL, Yueh B, Hannley MT, Johnson JT. Outcomes after nasal septoplasty: results from the Nasal Obstruction Septoplasty Effectiveness (NOSE) study. Otolaryngol. Head Neck Surg. 2004b; 130:283–290. [PubMed: 15054368]

Stewart MG, Witsell DL, Smith TL, Weaver EM, Yueh B, Hannley MT. Development and validation of the Nasal Obstruction Symptom Evaluation (NOSE) scale. Otolaryngol. Head Neck Surg. 2004a; 130:157–163. [PubMed: 14990910]

Sullivan CD, Garcia GJ, Frank-Ito DO, Kimbell JS, Rhee JS. Perception of better nasal patency correlates with increased mucosal cooling after surgery for nasal obstruction. Otolaryngol. Head Neck Surg. 2014; 150:139–147. [PubMed: 24154749]

Zhao K, Blacker K, Luo Y, Bryant B, Jiang J. Perceiving nasal patency through mucosal cooling rather than air temperature or nasal resistance. PLoS One. 2011; 6:e24618. [PubMed: 22022361]

Zhao K, Jiang J. What is normal nasal airflow? A computational study of 22 healthy adults. International forum of allergy & rhinology. 2014; 4:435–446. [PubMed: 24664528]

Zhao K, Jiang J, Blacker K, Lyman B, Dalton P, Cowart BJ, Pribitkin EA. Regional peak mucosal cooling predicts the perception of nasal patency. Laryngoscope. 2014; 124:589–595. [PubMed: 23775640]

Zhu JH, Lee HP, Lim KM, Gordon BR, Wang de Y. Effect of accessory ostia on maxillary sinus ventilation: a computational fluid dynamics (CFD) study. Respir. Physiol. Neurobiol. 2012; 183:91–99. [PubMed: 22750570]

Zhu JH, Lim KM, Thong KT, Wang de Y, Lee HP. Assessment of airflow ventilation in human nasal cavity and maxillary sinus before and after targeted sinonasal surgery: a numerical case study. Respir. Physiol. Neurobiol. 2014; 194:29–36. [PubMed: 24418355]

HIGHLIGHTS

- Spontaneous fluctuations in nasal mucosa engorgement are known as the nasal cycle.

- The nasal cycle confounds objective measures of nasal airflow.

- Simulations of nasal airflow were conducted in 12 patients pre- and post-surgery.

- Subjective scores of nasal patency were obtained pre- and post-surgery.

- To correct for the nasal cycle, virtual surgery was used to simulate airflow at mid-cycle.

- Correcting for the nasal cycle increases the correlation between objective and subjective measures of nasal airflow.
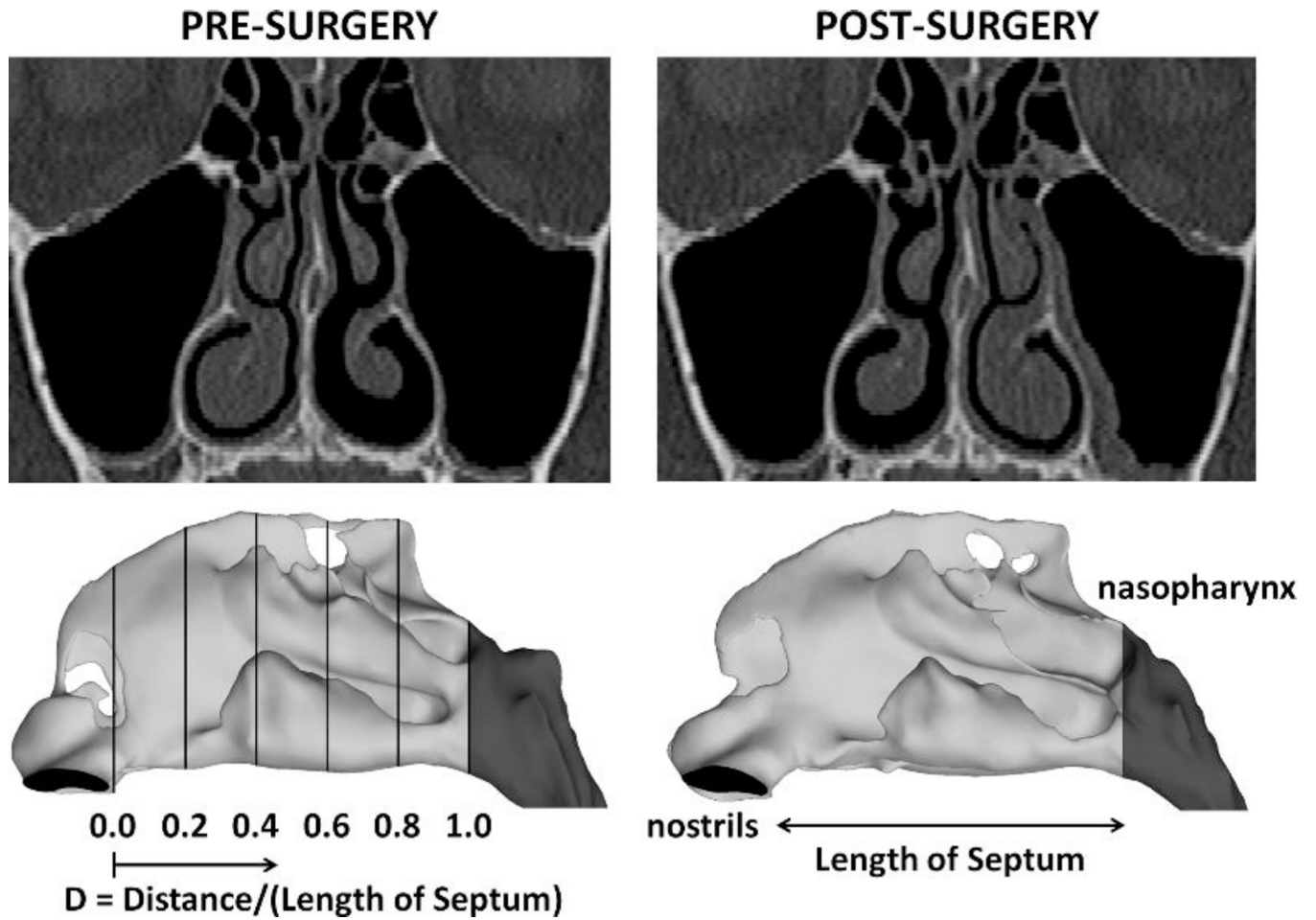
PRE-SURGERY

POST-SURGERY

Figure 1.

Pre- and post-surgery computed tomography scans illustrating reciprocal nasal mucosa changes due to the nasal cycle. The definition of the relative distance from nostrils (D) is displayed on a lateral view of the 3-dimensional models.
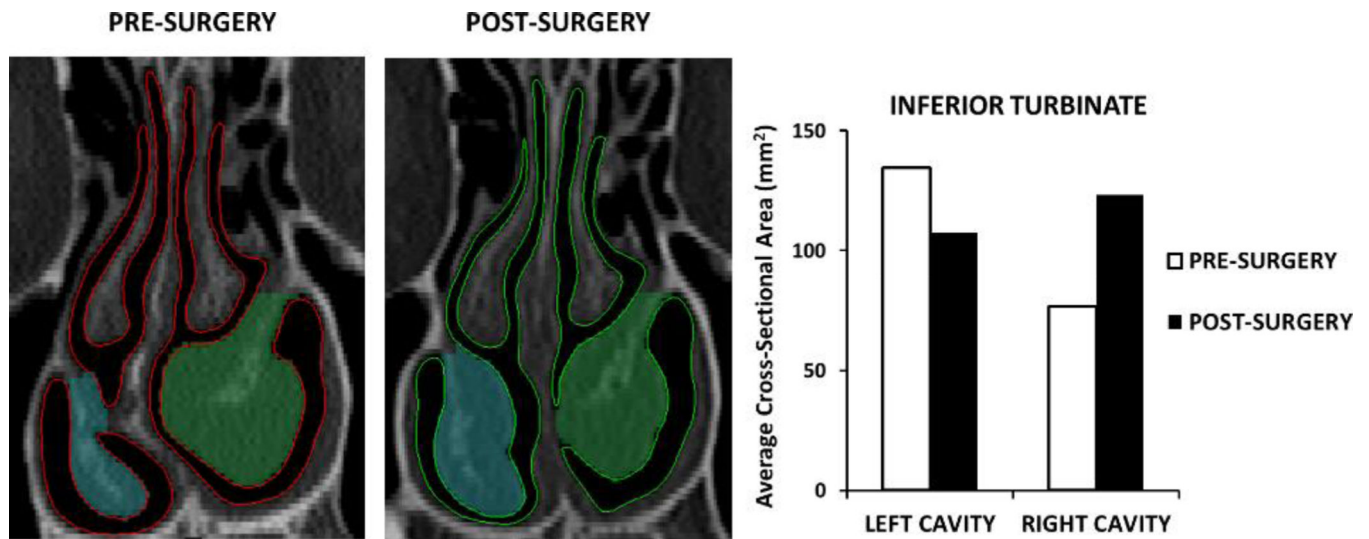
Figure 2.
Reciprocal changes in mucosal engorgement associated with the nasal cycle between pre- and post-surgery CT scans in one NAO patient who underwent septoplasty. The regions marked in blue and green on the CT scans represent the inferior turbinate cross-sectional area at this coronal section. The cross-sectional area of the inferior turbinate was averaged over 5 uniformly-spaced coronal sections located at 0.5 D 0.9 and used to select which patients exhibited nasal cycle changes between pre- and post-surgery CT scans.

NASAL PASSAGE MASKS

OUTLINES OF 3D MODELS

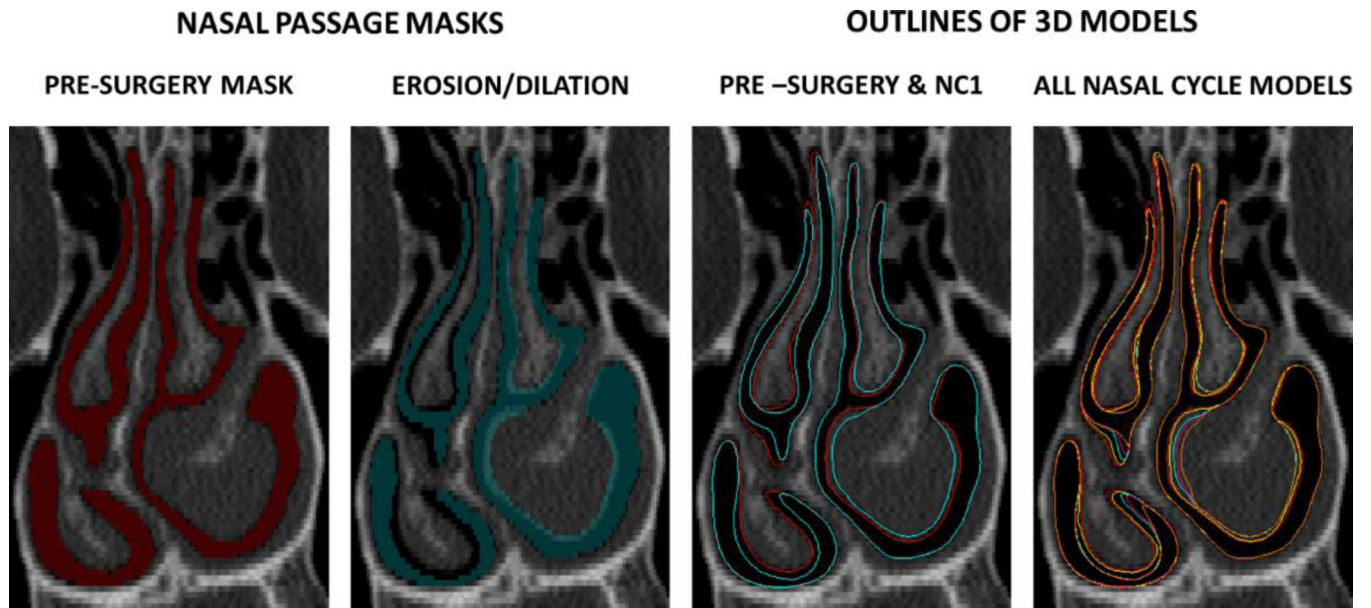| PRE-SURGERY MASK | EROSION/DILATION | PRE –SURGERY & NC1 | ALL NASAL CYCLE MODELS |

Figure 3.
Creation of nasal cycle models. The turbinates were reduced in the left cavity and dilated on the right cavity. This process was repeated in systematic steps to create several nasal cycle models (red=pre-surgery, yellow=NC1, blue=NC2, pink=NC3, orange=NC4). The NC1 model (yellow) represents the smallest change, while the NC4 model (orange) represents the greatest change as compared to the pre-surgery model.
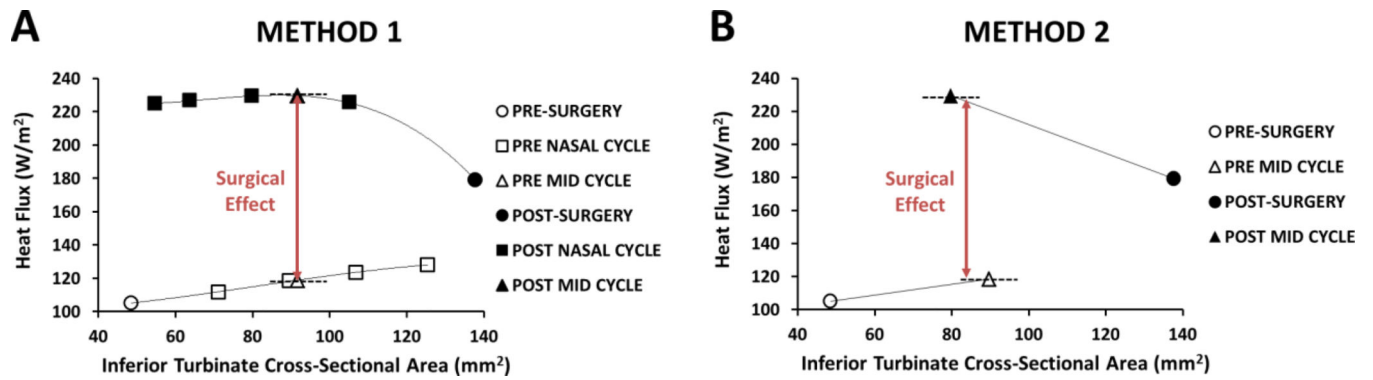
Figure 4.
Comparison of the two methods to estimate mid-cycle changes in objective measures of nasal airflow. (A) Method 1: Third order polynomial curves were fitted to the data and mid-cycle flow variables were estimated at the mid-cycle inferior turbinate cross-sectional area. (B) Method 2: A single mid-cycle model was created.
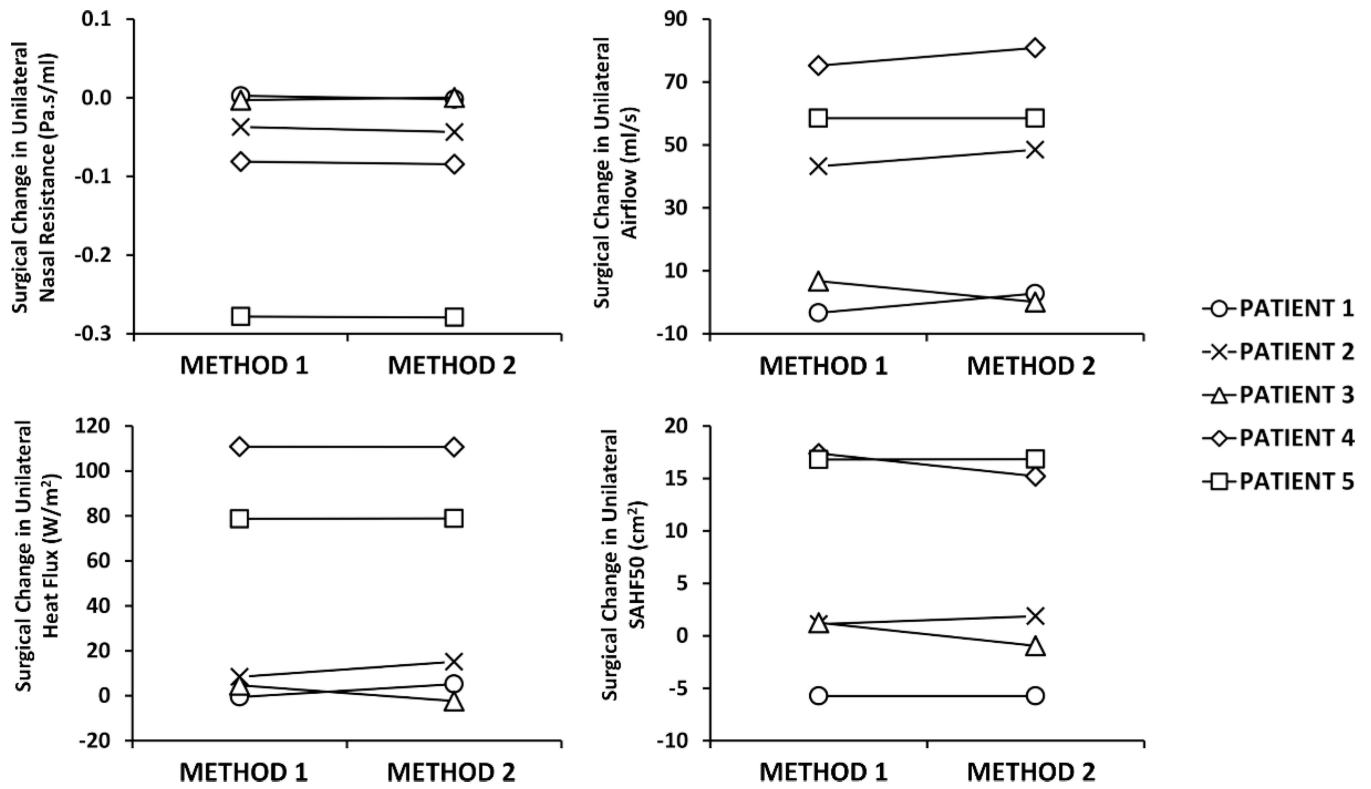
Figure 5.
Comparison of surgical change in unilateral variables estimated with Method 1 vs. Method 2 on the most obstructed side.
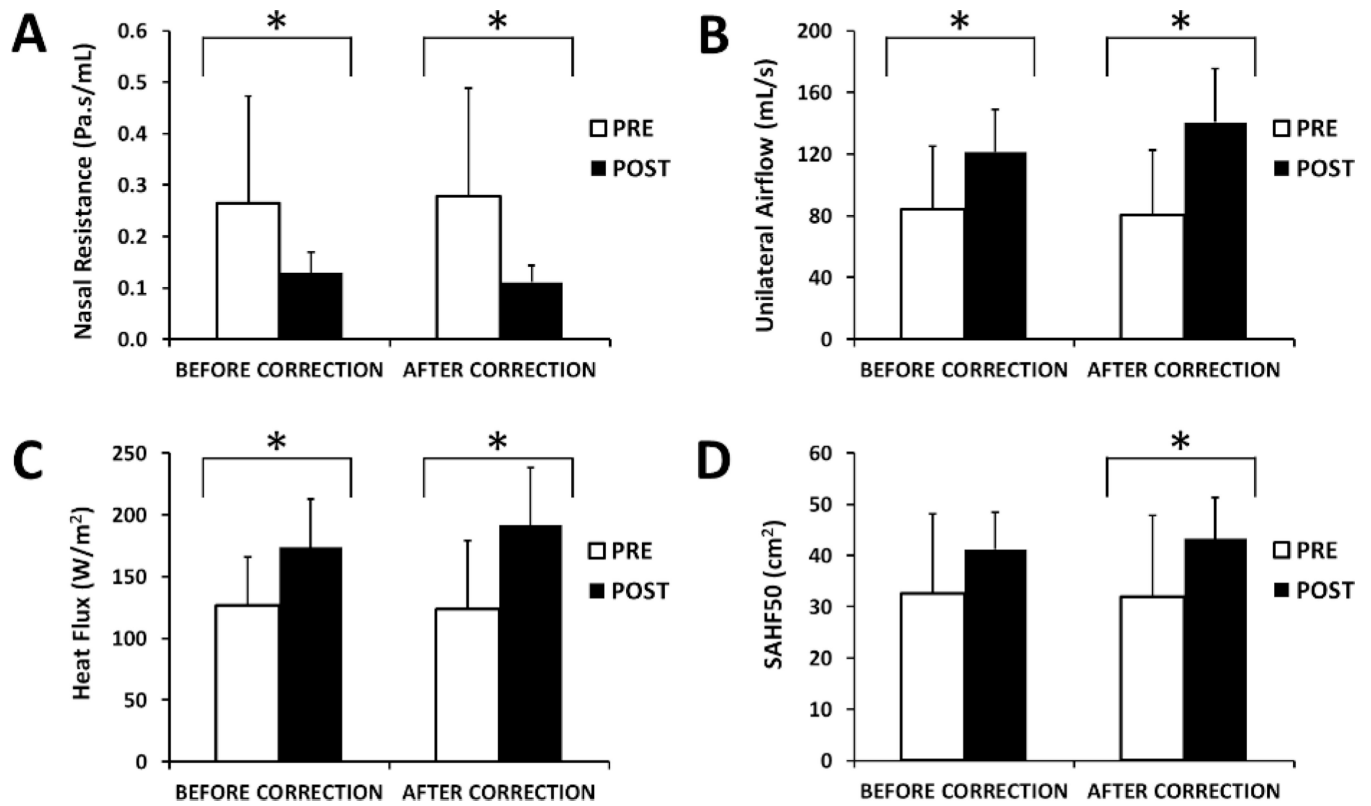
Figure 6.
Pre-surgery vs. post-surgery CFD variables measured unilaterally on the pre-operatively most obstructed side before and after correcting for the nasal cycle. * Statistically significant (p< 0.05).
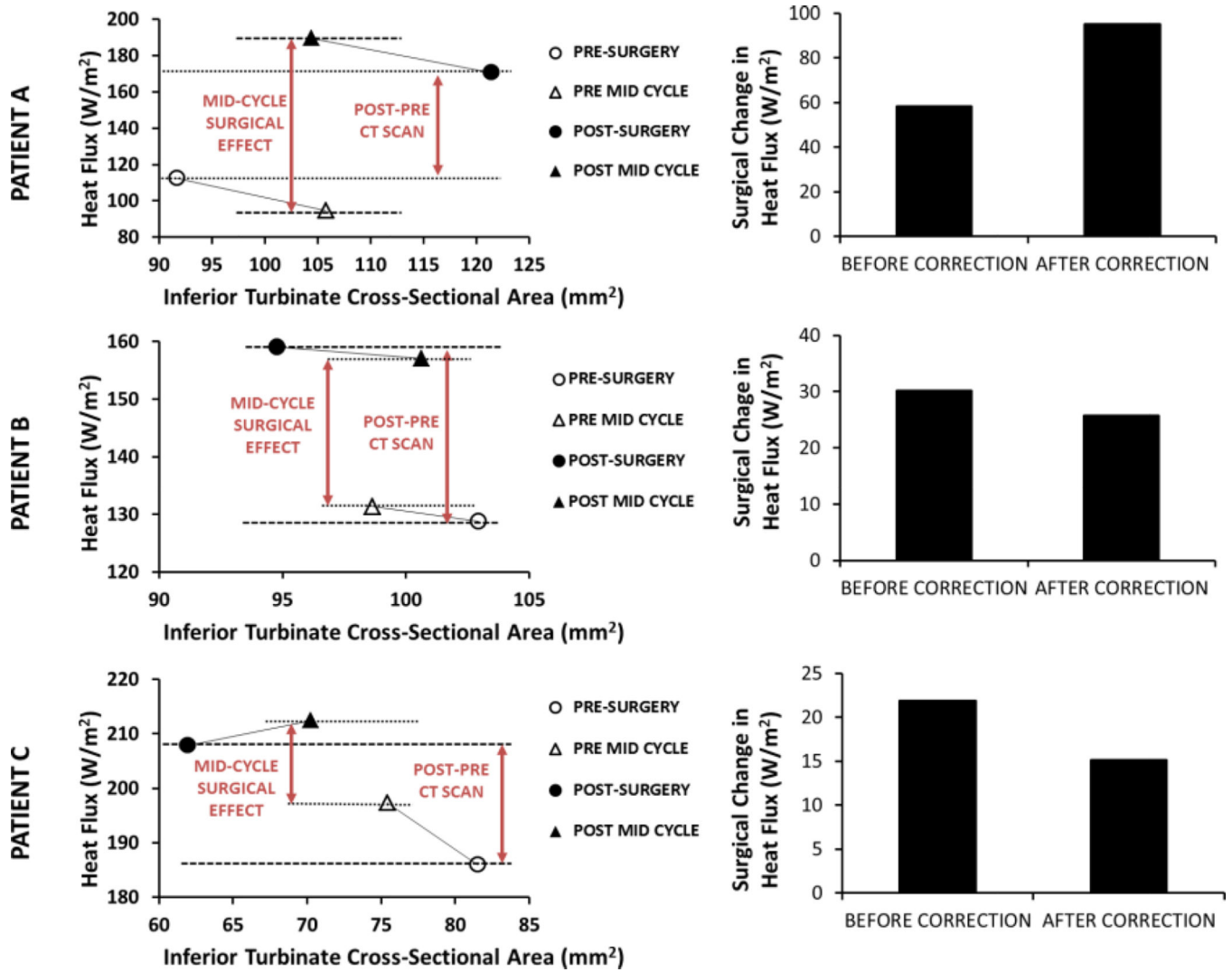
Figure 7.
Surgical changes in unilateral heat flux in the most obstructed nasal cavity of three NAO patients. Results are shown before and after correcting for the nasal cycle using Method 2.

BEFORE CORRECTION

A

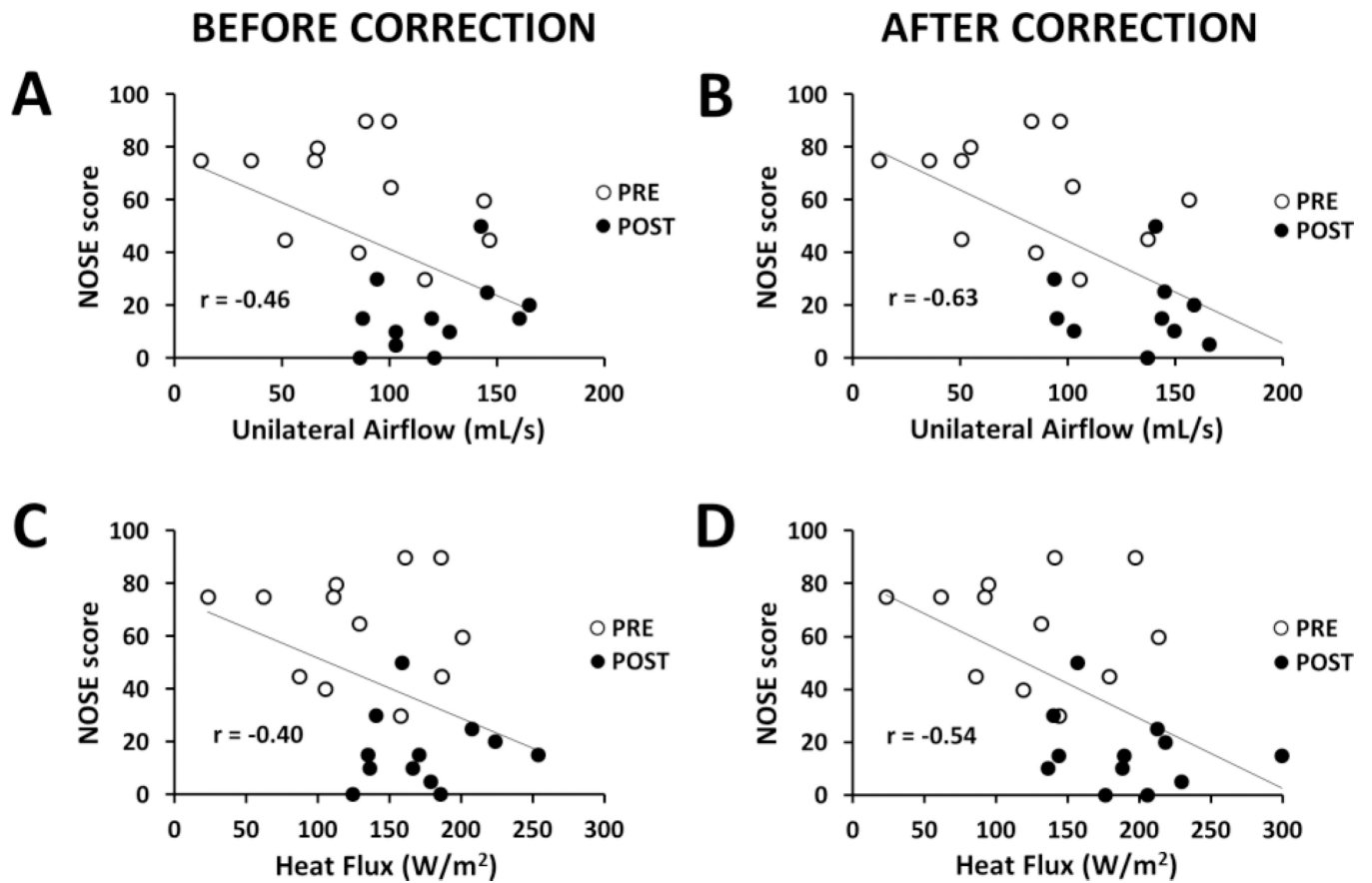## AFTER CORRECTION

B

C

D

Figure 8.
Correlations among subjective and objective measures of nasal airflow on the most obstructed side before and after correcting for the nasal cycle using Method 2.

Table 1

Percentage difference (see Equation (1)) between the results of Methods 1 and 2 in the 5 NAO patients on which both methods were performed.

CFD VARIABLE	PATIENT 1	PATIENT 2	PATIENT 3	PATIENT 4	PATIENT 5
NASAL RESISTANCE	0.4 %	7.6 %	5.0 %	6.9 %	0.7 %
FLOWRATE	2.2 %	3.6 %	1.4 %	0.1 %	0.8 %
HEAT FLUX	0.0 %	2.4 %	0.6 %	6.7 %	0.4 %
SAHF50	0.3 %	3.5 %	4.4 %	1.7 %	0.1 %

Abbreviations: SAHF50 = Unilateral surface area stimulated by mucosal cooling, defined as the mucosa surface area where heat fluxes exceed 50 W/m^2.

Table 2

Average unilateral CFD variables measured in the most obstructed side pre- and post-surgery. CFD variables are shown before and after correcting for the nasal cycle (NC) using Method 2.

CFD VARIABLE (most obstructed side)	BEFORE NC CORRECTION			AFTER NC CORRECTION		
	PRE	POST	p value	PRE	POST	p value
NASAL RESISTANCE (Pa.s/ml)	0.26 ± 0.21	0.13 ± 0.04	0.016 *	0.28 ± 0.21	0.11 ± 0.03	0.001 *
FLOWRATE (ml/s)	84 ± 41	121 ± 27	0.027 *	81 ± 42	141 ± 34	<0.001 *
HEAT FLUX (W/m^2)	127 ± 54	174 ± 39	0.027 *	124 ± 56	191 ± 47	0.001 *
SAHF50 (cm^2)	33 ± 15	41 ± 7	0.077	32 ± 16	43 ± 8	0.027 *

*
= statistically significant ($p < 0.05$) using Wilcoxon signed-rank test.

Table 3

Spearman correlation coefficients (r) and p values for the correlation of subjective nasal patency scores with unilateral CFD variables measured in the most obstructed side. Note that the correlation coefficients increased after correcting for the nasal cycle (NC) using Method 2.

CORRELATIONS (most obstructed side)	BEFORE NC CORRECTION		AFTER NC CORRECTION	
	r	p value	r	p value
NOSE				
FLOWRATE, ml/s	−0.41	0.048 *	−0.61	0.002 *
HEAT FLUX, W/m²	−0.31	0.144	−0.51	0.011 *
SAHF50, cm²	−0.29	0.173	−0.43	0.034 *
NASAL RESISTANCE, Pa.s/ml	0.32	0.128	0.55	0.005 *
VAS				
FLOWRATE, ml/s	0.40	0.052	0.56	0.004 *
HEAT FLUX, W/m²	0.34	0.102	0.51	0.011 *
SAHF50, cm²	0.22	0.303	0.38	0.068
NASAL RESISTANCE, Pa.s/ml	−0.36	0.087	−0.58	0.003 *

Abbreviations: NOSE = Nasal Obstruction Symptom Evaluation; VAS = visual analog scale; SAHF50 = surface area stimulated by mucosal cooling, defined as the mucosa surface area where heat fluxes exceed 50 W/m².

*
= statistically significant (p < 0.05).